SLAC–PUB–4931
March 1989
(E)

A MEASUREMENT OF THE RADIATIVE WIDTH OF THE η AND η' MESONS WITH THE ASP DETECTOR*

N. A. Roe,[a] G. Bartha,[b] D. L. Burke, P. Garbincius,[c]
C. A. Hawkins,[d] M. J. Jonker,[e] and T. R. Steele[f]
Stanford Linear Accelerator Center
Stanford University, Stanford, California 94309

and

A. S. Johnson, J. S. Whitaker, and R. J. Wilson
Boston University, Boston, Massachusetts 02215

and

C. Hearty,[a] J. E. Rothberg, and K. K. Young
University of Washington, Seattle, Washington 98195

and

R. J. Hollebeek
University of Pennsylvania, Philadelphia, Pennsylvania 19104

Formation of the η and η' mesons in two-photon interactions has been observed with the ASP detector at the SLAC e^+e^- storage ring PEP ($\sqrt{s} = 29$ GeV). In a data sample of 108 pb^{-1}, a total of 2287 η and 547 η' events have been detected in the $\gamma\gamma$ decay mode. The radiative widths are determined to be $\Gamma_{\gamma\gamma}(\eta) = 0.490 \pm 0.010 \pm 0.048$ keV, and $\Gamma_{\gamma\gamma}(\eta') = 4.96 \pm 0.23 \pm 0.72$ keV. The SU(3) pseudoscalar mixing angle deduced from these values is $\theta_p = -19.8 \pm 2.2°$.

Submitted to *Physical Review Letters*

---

*This work was supported in part by the Department of Energy contracts DE–AC03–76SF00515, DE–AC02–86ER40284, and DE–AC02–76ER03071, and by National Science Foundation Grant PHY–8503215.

[a] Present Address: Lawrence Berkeley Laboratory, Berkeley, California 94720
[b] Present Address: University of Southern California, Los Angeles, California 90007
[c] Present Address: Fermi National Laboratory, Batavia, Illinois 60510
[d] Present Address: ESL, Sunnyvale, California 94088
[e] Present Address: CERN, EP Division, Geneva, Switzerland CH–1211
[f] Present Address: Lightwave Electronics, Mountain View, California 94043

Two-photon interactions at e^+e^- storage rings provide the opportunity to study the formation of neutral resonances with positive charge conjugation. The coupling of a neutral meson to two photons via its constituent quarks is proportional to the fourth power of the quark charges. A measurement of the radiative width is therefore a probe of quark content, and can be used both to test theoretical predictions for established mesons and to aid in the identification of exotic states which do not fit into the meson nonet structure.

In the case of the light pseudoscalar mesons $\eta(549)$ and $\eta'(958)$, there is an explicit prediction for the radiative widths:[1]

$$\Gamma^{\eta}_{\gamma\gamma} = \frac{\alpha^2}{64\pi^3}\frac{M_\eta^3}{3}\left[\frac{1}{f_8}\cos\theta_p - \frac{\sqrt{8}}{f_1}\sin\theta_p\right]^2$$
$$\Gamma^{\eta'}_{\gamma\gamma} = \frac{\alpha^2}{64\pi^3}\frac{M_{\eta'}^3}{3}\left[\frac{1}{f_8}\sin\theta_p + \frac{\sqrt{8}}{f_1}\cos\theta_p\right]^2 \quad , \tag{1}$$

where f_1 and f_8 are the singlet and octet decay constants of the SU(3) basis states η_1 and η_8, analagous to the pion decay constant $f_\pi = 93$ MeV. The quark charges enter this prediction through the pseudoscalar mixing angle θ_p, which determines the quark content of the observed η and η' mass eigenstates in terms of the basis states of flavor SU(3):[2]

$$|\eta\rangle = \cos\theta_p|\eta_8\rangle - \sin\theta_p|\eta_1\rangle \quad , \qquad |\eta'\rangle = \sin\theta_p|\eta_8\rangle + \cos\theta_p|\eta_1\rangle \quad . \tag{2}$$

Thus a measurement of the radiative widths of the η and η' mesons provides a measure of θ_p.

In this experiment, η and η' mesons (denoted P collectively, for pseudoscalar), were produced in untagged two-photon interactions, and were observed in the $\gamma\gamma$

decay mode:

$$e^+e^- \rightarrow e^+e^-\gamma^*\gamma^* \rightarrow e^+e^-\mathrm{P} \quad , \qquad \mathrm{P} \rightarrow \gamma\gamma \quad . \tag{3}$$

The data sample of 108 pb^{-1} was collected at the PEP e^+e^- storage ring ($\sqrt{s}$ = 29 GeV) with the ASP detector. The ASP detector has been described in detail elsewhere;[3] the features of the detector which are relevant for this analysis are briefly summarized below.

The ASP detector is a non-magnetic, hermetic device which was designed for efficient detection of all-neutral final states over a large solid angle. The central calorimeter was constructed from 632 lead-glass bars of dimension $6\times6\times75$ cm^3, arranged in four quadrants. Each lead-glass bar had a photo-multiplier tube (PMT) glued to one end to detect Čerenkov light. The lead-glass calorimeter was 10 radiation lengths thick at normal incidence and had an energy resolution given by $\sigma_E = 10\%\sqrt{E}$ (E in GeV). Interleaved with the lead glass were five layers of proportional wire chamber (PWC) oriented orthogonally to the lead-glass bars. A central tracker inside the lead-glass calorimeter consisting of five layers of drift tubes provided charged-track identification. A time-of-flight (TOF) system, consisting of scintillator paddles suspended from the ceiling above the lead-glass calorimeter, was used primarily to reject cosmic ray events. Two forward calorimeter modules constructed from lead-scintillator sandwich were located on each side of the interaction point (IP), extending the coverage to within 21 mr of the beamline.

Photon trajectories were reconstructed by combining the showers in the lead-glass bars and the central PWC's; the lead-glass bars measured θ_{prj}, while the central PWC's measured ϕ. (θ_{prj} is the polar angle θ projected onto the plane containing the beam, normal to the lead-glass bars.) The errors on the reconstructed trajectories for tracks of .5 to 5 GeV are given by $\sigma_{\theta_{prj}} = 4.4°$ and $\sigma_{\phi} = 3.2°$.

The physics triggers[4] were based on sums of the PMT signals from the lead-glass calorimeter, including the total energy, quadrant sums and layer sums. The most important trigger for this analysis required approximately .7 GeV of total lead-glass energy deposited within ± 20 ns of the beam crossing, with at least .15 GeV in the back four layers of one quadrant or of two opposite quadrants. In addition, diagnostic triggers recorded events from radiative Bhabha and low-angle Bhabha events, cosmic rays and randomly selected beam crossings.

The event selection procedure required two neutral showers ('photons') within the acceptance of the lead-glass calorimeter, $20° \leq \theta_{prj} \leq 160°$. Both θ_{prj} and ϕ were required to be well-measured. To reduce the systematic error resulting from uncertainty in the trigger efficiency, a software trigger cut was imposed on the raw signal from the lead-glass calorimeter at a threshold corresponding to approximately 700 MeV of energy. The event was then vetoed if there was: (1) more than 25 MeV of stray energy in the lead glass; (2) more than 150 (300) MeV of energy in the inner (outer) forward calorimeters; (3) time-of-flight information consistent with a cosmic-ray event; (4) a pattern of energy deposition in either the lead glass or the central PWC system that was either narrow and uniform, consistent with a minimum-ionizing track, or broad, consistent with two overlapping photons from the decay of a $\pi°$; (5) more than 20 GeV of visible energy and an acolinearity of less than 10°. Finally, the acoplanarity angle (the difference in azimuthal angle) between the two photons was required to be greater than 135°, and the net p_t, defined as the vector sum of transverse momenta, was required to be less than

300 MeV/c. The net p_t distribution before these last two cuts were applied is shown in Fig. 1 for all events with invariant mass less than 2 GeV/c^2; it is sharply peaked toward low p_t, as expected for two-photon interactions.

The $\gamma\gamma$ invariant mass spectrum of the final data sample is shown in Fig. 2. Clear peaks are evident at the η and η' masses. Some background due to two-photon production of the $f_2(1270)$, a tensor meson which has a large decay rate to $\pi^\circ\pi^\circ$, is visible above the η'. These events may pass the event selection criteria if the two photons from the π° decay overlap or if one is undetected. (The f_2 peak is shifted down from the nominal mass due to the falling $\gamma\gamma$ flux and because low energy photons from the π° decays may go undetected.)

The fit to the data (see Fig. 2) consists of the sum of two Gaussians with power-law tails to describe the η and η', and a Breit–Wigner with total width of 176 MeV/c^2 convoluted with a Gaussian to describe the f_2. The form of the fitting function was determined using Monte Carlo data samples which had passed all event selection criteria. The mean and width of the η' and the f_2 were then fixed according to the results of the Monte Carlo simulation, because these parameters were highly correlated in the fit. The parameters describing the power-law tails of the η and η' were also fixed. The number of events in each peak was a free parameter, as were the mean and width of the η peak. Systematic errors for the fit were determined by simultaneously varying the fixed parameters. The number of η events determined by the fit is $2380 \pm 49(\text{stat.}) \pm 25(\text{sys.})$, with a mean invariant mass of 545 ± 1.3 MeV/c^2 and a width of 57 ± 1.2 MeV/c^2, in good agreement with the results of Monte Carlo simulation, and in reasonable agreement with the nominal η mass[5] of 548.8 ± 0.6 MeV/c^2. The number of η' events is determined to be 568±26(stat.)±56(sys.), where the systematic error is dominated by uncertainty in the contribution from the f_2. The χ^2 probability of the combined fit is 47%.

The radiative width is extracted from the fitted $\gamma\gamma$ invariant mass spectrum according to:

$$\Gamma^{P}_{\gamma\gamma} = \frac{\mathrm{N}}{\tilde{\sigma} \cdot \mathcal{L} \cdot \epsilon \cdot \mathrm{Br}(P \to \gamma\gamma)} \quad . \tag{4}$$

In this expression, P refers to either the η or η', and $\Gamma^{P}_{\gamma\gamma}$ is the radiative width in keV. The quantities on the right-hand side of Eq. 4 are summarized in Table 1, and their determination is discussed below.

Table 1. Summary of the quantities necessary for the calculation of the radiative width of the η and η'.

	η	η'
Events from fit	$2380 \pm 49 \pm 25$	$568 \pm 24 \pm 56$
Background	93 ± 51	21 ± 4
Events – Background	$2287 \pm 49 \pm 57$	$547 \pm 24 \pm 56$
$\tilde{\sigma}$ (nb/keV)	$2.560 \pm .051$	$.362 \pm .007$
Efficiency	$.043 \pm .004$	$.131 \pm .008$
Luminosity (pb^{-1})	108.0 ± 1.4	108.0 ± 1.4
$\gamma\gamma$ branching ratio	$.389 \pm .004$	$.0216 \pm .0016$

The production cross section is given by the product $\tilde{\sigma} \cdot \Gamma^{P}_{\gamma\gamma}$; thus $\tilde{\sigma}$ has units of nb/keV. This quantity has been calculated using a QCD form-factor[6]; as an estimate of the uncertainty in $\tilde{\sigma}$ we take the difference in the accepted cross section with and without the form factor. The integrated luminosity, $\mathcal{L} = 108\ \mathrm{pb}^{-1}$, was determined using low-angle Bhabha scatters. $\mathrm{Br}(X \to \gamma\gamma)$ is the branching ratio into two photons, which in the case of the η and η' is known from fixed target experiments.[5]

N is the number of background-corrected events of each type; backgrounds which have been calculated include the fourth-order QED processes $e^+e^- \rightarrow e^+e^-\gamma\gamma$ and $e^+e^- \rightarrow e^+e^-e^+e^-$, where the electrons are mis-identified as neutral, the two-photon processes $\gamma\gamma \rightarrow a_2(1320) \rightarrow \eta\pi^\circ$ and $\gamma\gamma \rightarrow \pi^\circ\pi^\circ$ in the continuum, as well as cosmic-ray and beam-gas backgrounds. The only significant background contributions in the η region are from continuum $\gamma\gamma \rightarrow \pi^\circ\pi^\circ$ production and from beam-gas interactions. The former has been estimated using Monte Carlo simulation and recent experimental data[7] to be 37 ± 19 events. The latter was estimated both by selecting events produced away from the interaction point in $\hat{z}$ and by direct calculation.[8] The two methods were in good agreement, although both had large errors; the average result was 53 ± 47 events. In the η' region, the dominant background from the $f_2(1270)$ is determined by the fit to the data. The other backgrounds in the η' region, which are all small and contribute about equally, are $e^+e^- \rightarrow e^+e^-\gamma\gamma$, and two-photon production of $a_2 \rightarrow \eta\pi^\circ$ and $\pi^\circ\pi^\circ$ in the continuum.

The efficiency, ϵ, is given by the product of the detector acceptance, the trigger efficiency, and the event selection efficiency. These factors were determined using Monte Carlo-generated samples of η and η' events[9] with an equivalent integrated luminosity about seven times greater than that of the data. The events were passed through a detailed detector simulation routine based on the EGS electromagnetic shower simulation program.[10] The detector acceptance, which is determined by requiring two photons in the region $20^\circ < \theta_{prj} < 160^\circ$ and no electron scattered above 21 mr, was $25.9 \pm 0.9\%$ for $\eta \to \gamma\gamma$ events and $30.6 \pm 0.9\%$ for $\eta' \to \gamma\gamma$ events.

The trigger efficiency was determined using a detailed trigger simulation which included threshold effects, dead channels and attenuation of Čerenkov light in the lead-glass bars. The software trigger cut at 700 MeV was also imposed; above this energy the trigger efficiency was high and fairly flat. The combined hardware and software trigger efficiency for events within the detector acceptance was $40.9 \pm 2.4\%$ for the η and $94.7 \pm 1.1\%$ for the η'.

The trigger efficiency was much lower for η events because the trigger threshold was above the η mass of 549 MeV; only those events in which the η was produced with a longitudinal boost satisfied the trigger. The effect of the trigger on η events can be seen in Fig. 3(a). The data points show the total energy distribution of η events from the final $\gamma\gamma$ data sample (.4 GeV$< M_{\gamma\gamma} <$ .7 GeV), without the software trigger imposed. The solid histogram represents Monte Carlo simulation for the same requirements. The dashed histogram is Monte Carlo simulation without either the hardware or software triggers imposed. The loss in efficiency due to the hardware trigger is clearly evident; the good agreement between the data points and the solid histogram indicate that the trigger simulation is quite accurate. The systematic error on the trigger efficiency was determined by a similar comparison using a data sample of 2.2×10^5 untagged events from the fourth-order QED process $e^+e^- \to (e^+e^-)e^+e^-$. In this high statistics study, the total energy distribution of the Monte Carlo simulation reproduced the data very well, as shown in Fig. 3(b).

The efficiency of the event selection criteria for events within the detector acceptance which also satisfied the trigger was $41.0 \pm 2.4\%$ and $45.0 \pm 2.6\%$ for η and η' events, respectively. Uncertainties in detector simulation were the dominant source of systematic error; they have been determined by detailed comparison of Monte Carlo simulation with data.

Using Eq. (4) and the results summarized in Table 1 yields the following results for the radiative widths:

$$\Gamma_{\gamma\gamma}(\eta) = 0.490 \pm 0.010 \pm 0.048 \text{ keV}$$

$$\Gamma_{\gamma\gamma}(\eta') = 4.96 \pm 0.23 \pm 0.72 \text{ keV} \quad ,$$

where the first error is statistical and the second is systematic. The pseudoscalar mixing angle calculated using Eq. (1) is $\theta_p = -19.8 \pm 2.2°$. The singlet decay constant is determined to be $f_1 = (1.02 \pm .14)f_\pi$. In this calculation we have not assumed nonet symmetry; the near equality of f_1 and f_π comes out naturally. To solve Eq. (1) we have used $f_8 = 1.25 f_\pi$, based on a calculation which incorporates SU(3) symmetry breaking at the one-loop level in chiral perturbation theory,[11] and have assigned a theoretical error of 5% on this calculation.[2]

This value of θ_p is also in agreement with the pseudoscalar mixing angle calculated using the Gell-Mann–Okubo mass formula, provided SU(3) breaking effects are also incorporated in this calculation.[10] Thus a consistent picture of mixing in the pseudoscalar meson nonet has emerged based on recent experimental evidence and theoretical calculations.

We acknowledge useful discussions with F. Gilman and R. Kauffman, and constructive criticism of the manuscript by P. Extermann. We thank D. Chambers,

R. Baggs, D. Forbush, L. Keller, T. Lyons, C. Matteuzzi, C. Noyer, K. Skarpass, and R. Stickley for considerable technical assistance with the construction and installation of the detector. We are also grateful to the PEP operations staff.

REFERENCES

1. S. Adler, Phys. Ref. **177**, 2436 (1969); J. S. Bell and L. Jakiw, Nuovo Cim. **60**, 47 (1969).

2. For a summary of SU(3) formalism and a review of current experimental results on θ_p, see F. Gilman and R. Kauffman, Phys. Rev. **D36**, 2761 (1987).

3. G. Bartha *et al.,* Nucl. Inst. & Meth., **A275**, 59 (1989).

4. R. J. Wilson, *Proceedings of the Workshop on Triggering, Data Acquisition and Computing for High Energy/High Luminosity Hadron-Hadron Colliders*, eds. B. Cox, R. Fenner and P. Hale, 118 (1986).

5. G. P. Yost *et al.* (Particle Data Group), Phys. Lett. **204B**, 1 (1988).

6. S. Brodsky and P. Lepage, Phys. Rev **D24**, 1808 (1981).

7. H. Marsiske, Ph.D. thesis, Hamburg University, July, 1988 (unpublished).

8. For more details, see N. A. Roe, Ph.D. thesis, Stanford University, 1989, SLAC–0388.

9. J. Vermaseren, Nucl. Phys. **B229**, 347 (1987).

10. R. L. Ford, W. R. Nelson, SLAC–PUB–0210, June 1978.

11. J. Donoghue, B. Holstein and Y. Lin, Phys. Rev. Lett. **55**, 2766 (1985).

FIGURE CAPTIONS

1) Net transverse momentum distribution of final $\gamma\gamma$ sample.

2) Invariant mass distribution of the final $\gamma\gamma$ sample. The solid line is the combined fit; the dashed line shows the η' and f_2 contributions.

3) (a) Total energy distribution for $\eta \to \gamma\gamma$ events. The dashed curve is Monte Carlo simulation with no trigger imposed; the histogram is the same with the trigger requirement. The points are η events from the final $\gamma\gamma$ data sample. (b) Total energy distribution for untagged $e^+e^- \to (e^+e^-)e^+e^-$ events. The histogram is Monte Carlo simulation with the trigger requirement imposed; the points are data.

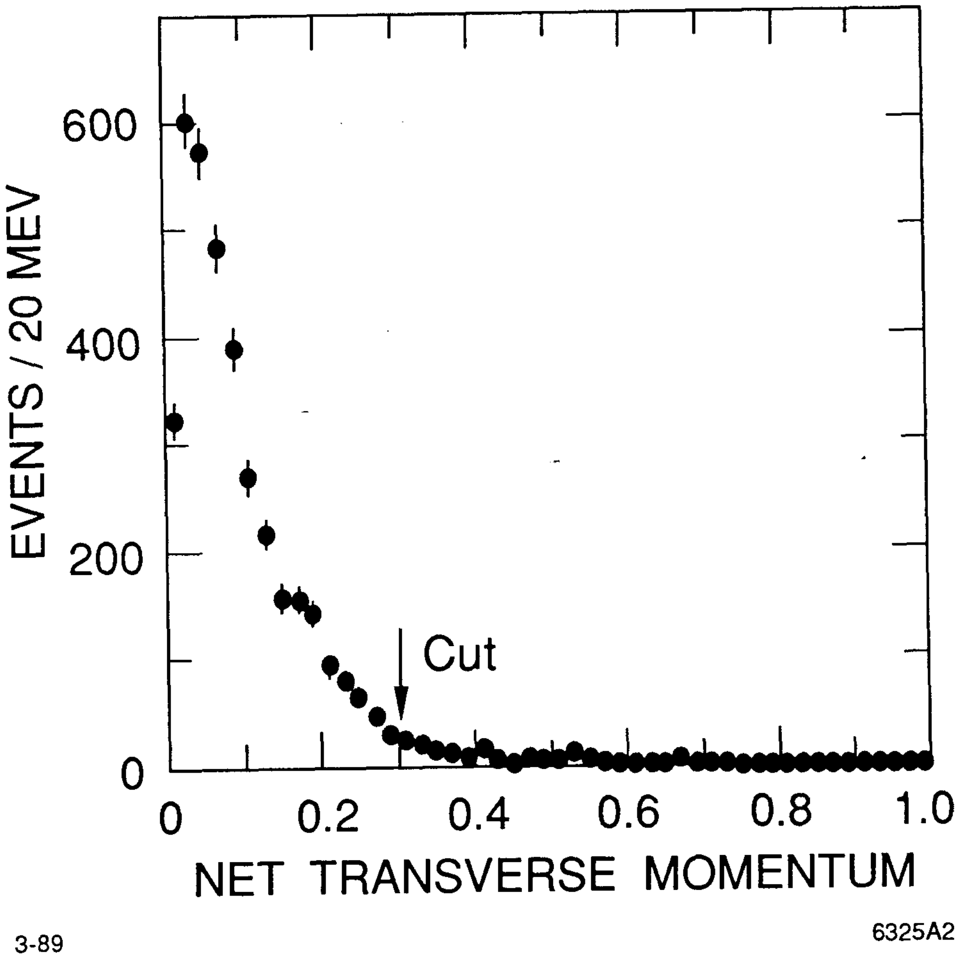
600
400
200
0
EVENTS / 20 MEV
Cut
0
0.2
0.4
0.6
0.8
1.0
NET TRANSVERSE MOMENTUM
3-89
6325A2

Fig. 1

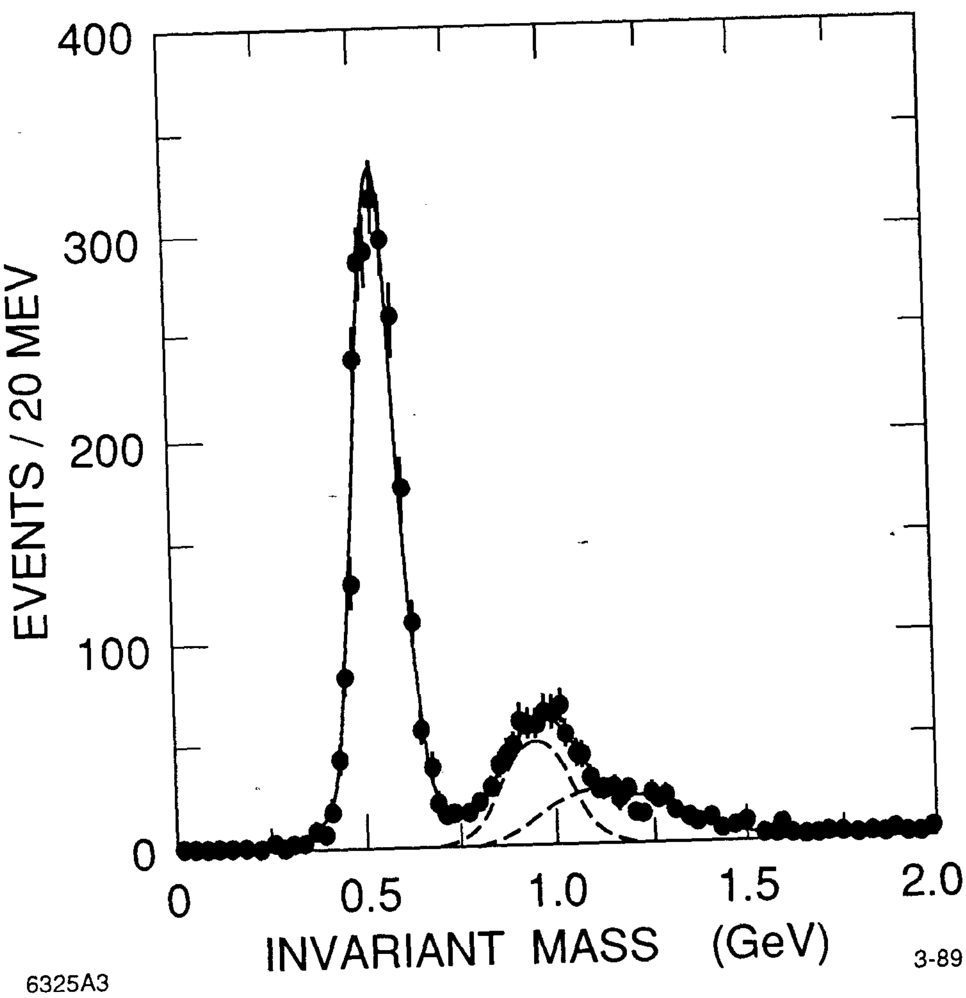
400
300
200
100
0
EVENTS / 20 MEV
0
0.5
1.0
1.5
2.0
INVARIANT MASS (GeV)
6325A3
3-89

Fig. 2

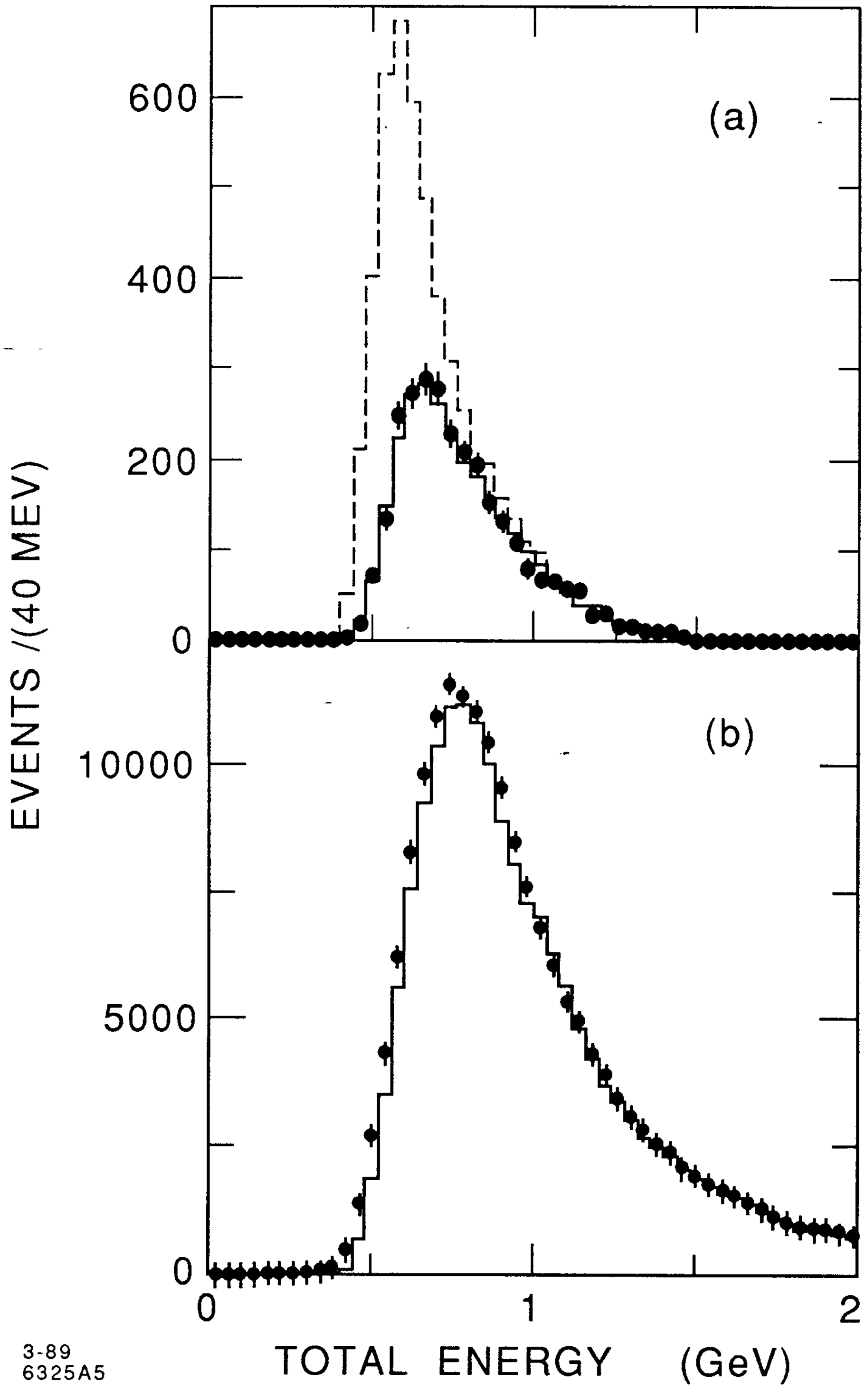

3-89
6325A5

Fig. 3